Appl. Phys. B 34, 207–219 (1984)

Applied Physics B Photophysics and Laser Chemistry

Optical Klystron Experiments for the ACO Storage Ring Free Electron Laser

D. A. G. Deacon[1], M. Billardon[2], P. Elleaume[3], J. M. Ortega[2], K. E. Robinson[4], C. Bazin, M. Bergher, M. Velghe[5], J. M. J. Madey[4], and Y. Petroff

L.U.R.E., L.P. CNRS 008, Bâtiment 209-C,
Université de Paris-Sud, F-91405 Orsay, France

Received 2 January 1984/Accepted 20 March 1984

Abstract. To improve the gain in the Orsay storage ring Free Electron Laser (FEL) experiment, the 17 period permanent magnet undulator has been modified to form an optical klystron (OK). We report the measurement of spontaneous emission and the effects on it of energy spread and angular spread. Gain and laser induced bunch lengthening measurements with the OK are also reported and are in very good agreement with the FEL classical theory. The spontaneous emission spectrum which is easy to measure with good signal to noise ratio, turns out to be a very good diagnostic tool for *energy spread and angular spread measurements* on storage rings. The factor of four increase in the small gain obtained by converting the undulator NOEL into an OK was the critical factor in the recent operation of the ACO storage ring laser above threshold.

PACS: 42.60, 42.55

The main purpose of the Orsay experiment is to prove the feasability and test the theories of a storage ring free electron laser (FEL) in the visible range. A permanent magnet undulator has recently been built [1, 2] and has successfully operated on the electron storage ring ACO in the energy range 150–540 MeV [3]. However ACO is not optimized for FEL studies. The relatively low electron density (for storage rings) and the short length of the available straight section have conspired to limit the gain available with an undulator to 1 to $2\,10^{-4}$ per pass at a wavelength $\lambda = 6300\,\text{Å}$ and 240 MeV electron energy. Even with state-of-the-art mirrors, laser operation is impossible at this level of gain. Several directions have been followed to improve the gain. The most successful approach has been the modification of the undulator into an optical klystron (OK). In this paper we shall discuss our experience with the OK. The OK originally proposed by Vinokurov and Skrinsky [4] consists of two identical undulators separated by a dispersive section forcing the electron into a single large wiggle (Fig. 1). This configuration has a higher gain than an undulator of the same total length. Such a device can be used to advantage on electron beams with energy spread and it allows the maximization of the gain in an interaction region of fixed length.

Early results have already been reported [3]. In this paper we report on the dispersive section optimization (Sect. 1), spontaneous emission measurements (Sect. 2), gain measurements (Sect. 3) and laser induced bunch lengthening (Sect. 4). The spontaneous emission results are very detailed because they are easy to measure with a good signal to noise ratio and give much information on the OK FEL behaviour.

We use the notation of the theoretical description of optical klystrons of [5].

Permanent addresses:
[1] Deacon Research, 754 Duncardine Way, Sunnyvale, CA 94087, USA
[2] Ecole Supérieure de Physique et Chimie, 10, rue Vauquelin, F-75231 Paris Cedex 05, France
[3] Département de Physico-Chimie, Service de Photophysique, CEN Saclay, F-91191 Gif-sur-Yvette, France
[4] High Energy Physics Laboratory, Stanford University, Stanford, CA 94305, USA
[5] Laboratoire de Photophysique Moléculaire, Bâtiment 213, Université de Paris-Sud, F-91405 Orsay, France

1. Optimization of the Dispersive Section

The original 17 periods undulator NOEL [1] was desined to allow the replacement of the central 3 periods by a dispersive section. This operation converts NOEL into an optical klystron.

The OK gain results from the competition of two effects: a) the gain is decreased by removing the central periods (by a factor of about 0.56 for the retained solution); and b) the gain is improved by inserting the dispersive section (by a factor of about 10). The best optical klystron for a given pole face gap would have a very high field dispersive section occupying the smallest possible lengh. The dispersive section design problem is therefore closely connected with the undulator design problem (minimizing the period for a given gap and field). The most efficient technologies are known to be superconductivity and permanent magnets.

The decision was made to build the dispersive section with the same type of permanent magnets used for the undulator [1] (dimensions $50 \times 19 \times 19\,\text{mm}^3$, remanent field ~ 0.85 T, from BBC-Recoma) for two main reasons: a high enough magnetic field was impossible to achieve with regular electromagnets without an expensive water cooling system, and the use of the same technology as for the undulator sharply reduced the construction time. The permanent magnet system has the disadvantage of having a constant field which can only be changed by adjusting the gap between the jaws. The use of the same mechanical system for undulator and dispersive section couples both field variations with the gap and only permits a one-time adjustment of the relative amplitude. This is not very important since the optical klystron will remain optimized in a large range of magnetic gaps.

As in the case of the undulator, the magnets were individually measured, paired and glued into $100 \times 19 \times 19\,\text{mm}^3$ bars to compensate for the horizontal component of the field [2]. We have studied the configuration of $\{n/2,\ 6-n,\ 6-n,\ n/2\}$ magnet elements arranged vertically and horizontally as $+V$, $+H$, $-V$, $-H$, $+V$ respectively (see Fig. 2 which presents two layers of such a configuration for $n=3$). This configuration was chosen because if n is an integer, the smallest magnet element is a half pole, the above distribution gives twelve elements, and is automatically compensated for orbit angle and position deviations since the field integral is zero and the field is symmetric with respect to the middle.

The magnetic field was calculated using an electrostatic-like potential calculation code described in [1]. For each configuration we calculated N_d the dimensionless parameter that determines spontaneous emission spectrum and gain [5]. N_d represents the number of periods of light of wavelength λ passing over an electron which total energy is γmc^2 in the dispersive section. For light propagating on the axis of the dispersive section it reads (in SI units):

$$N_d = \frac{1}{2\lambda\gamma^2}\left[d + \frac{e^2}{m^2c^2}\int_{-\infty}^{\infty}\left[\int_{-\infty}^{u} B(z)dz\right]^2 du\right], \tag{1}$$

where m is the electron mass, e the electron charge, c the speed of light, d is the dispersive section length (12 magnets long) and $B(z)$ the vertical magnetic field created by the dispersive section magnets at the longitudinal coordinate z. $B(z)$ and therefore N_d are calculated on and off the axis of the dispersive section. The Table 1 gives the calculated on axis N_d at $\lambda = 6328$ Å, $\gamma mc^2 = 240$ MeV for one layer of magnets with a remanent field of 0.85 T and a gap of 32 mm. The optimal value of $n=3$ was chosen for our system. Table 2 shows N_d for $n=3$ and m layers of magnets. We have also calculated σ_γ/γ the corresponding relative energy spread for which the OK gain would be optimized, using (4).

$$N_d = \frac{1}{4\pi\sigma_\gamma/\gamma} - N, \tag{2}$$

where $N=7$ is the number of periods of one of the two identical undulators constituting the optical klystron.

Since the ACO energy spread is close to 10^{-3} at nominal current, we chose $m=2$. Figure 2 shows the retained configuration.

Table 1

n	0	1	2	3	4	5	6
N_d	20.1	25.3	29.9	32.7	31.2	26.0	18.4

Table 2

m	N_d	σ_γ/γ
1	32.7	2×10^{-3}
2	79	9.3×10^{-4}
3	114	6.6×10^{-4}

Each magnet of the external layer (the one farthest from the electron beam) was individually glued on an aluminium piece that was clamped on a bench as for the undulators. Magnets of the internal layers were glued to those of the external layers. The two jaws were made as symmetric as possible and the strongest magnets were placed on the ends to allow final orbit compensation by moving these adjustable magnets

away from the axis of the electron beam (Fig. 2). The calculated trajectory is shown in Fig. 1 which shows a large wiggle of about 2 mm amplitude for an electron energy of 240 MeV and a gap of 33 mm.

2. Spontaneous Emission

2.1. General Features of the Fundamental

As was done for the undulator, the electron beam is initially aligned by optical means into the axis of the vacuum chamber within ± 1 mm [3].

The spontaneous emission pattern of the optical klystron looks the same to the eye as that of an undulator [7, 6, 3], namely a series of concentric coloured rings with a similar pattern produced by each harmonic at progressively larger opening angles. The big difference appears in the spectrum.

The experimental set up used to measure the spontaneous emission spectrum has already been described [6]. It consists of a 1750 mm focal length spherical mirror placed at about 6.5 m from the center of the optical klystron.

The light transmitted by a 75 μm pinhole placed at the focal distance from the mirror is sent through a lens into an M20 uv Jobin Yvon monochromator (4 Å resolution with 0.1 mm slits). The output of the monochromator is then sent into a Hamamatsu R 928 photomultiplier. Fig. 3 shows a spontaneous emission spectrum of the fundamental at an energy of 240 MeV for a gap of 34.4 mm at low current in the ring.

We have compared the envelope of the oscillations with that of the emission spectrum of a perfect undulator having exactly N sinusoidal periods, the fields outside these periods being exactly zero. The emission spectrum $dI/d\lambda$ of such an undulator is:

$$\frac{dI}{d\lambda} \alpha \frac{1}{\lambda^4} \left(\frac{\sin \delta}{\delta} \right)^2 \tag{3}$$

with $\delta = n\pi N (1 - \lambda_R/\lambda)$,

where λ_R is the resonant wavelength and n is the harmonic number. Fitting the envelope to curves given by (3) gives $N = 8.1 \pm 0.1$ instead of 7. This discrepancy is probably due to the dispersive section field which could be partly resonant with the other 7 periods. It is certainly not due to the fringe field of the half periods which slightly decreases the effective number of periods. The envelope of oscillations also presents a long, short wavelength tail with the secondary maximum amplitude lower than expected. This effect was also seen in the 17 period undulator emission curves and is due to the parasitic tail of the ACO bending magnets fringe field [2]. Similar curves of emission were obtained as function of energy or field in the dispersive section (by changing the gap).

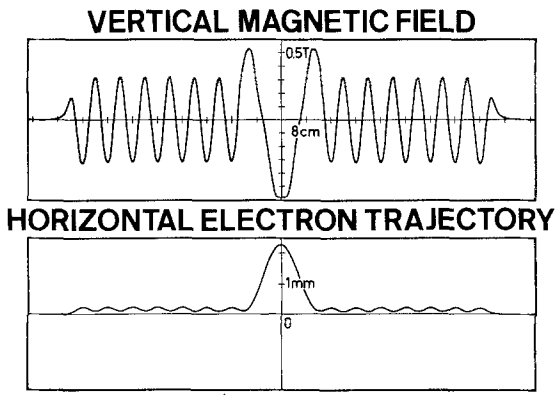

Fig. 1. Vertical magnetic field calculated for the Orsay optical klystron (gap: 33 mm) and the corresponding calculated horizontal electron trajectory at an energy of 240 MeV

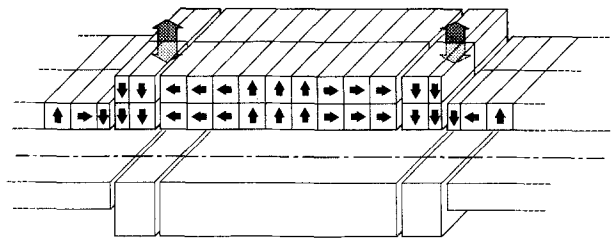

Fig. 2. Dispersive section permanent magnet configuration optimizing the low field gain

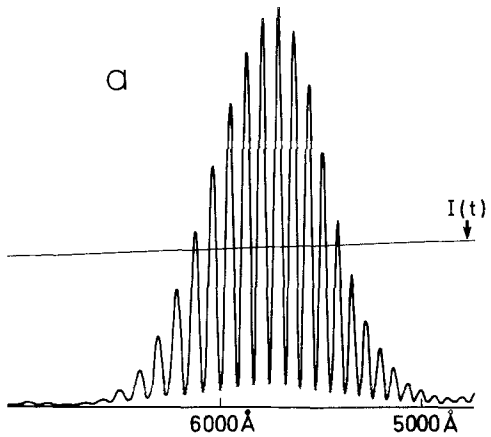

Fig. 3. Spontaneous emission spectrum $dI/d\lambda d\Omega$ measured for an electron energy of 238 MeV and a magnetic field parameter of $K = 2.09$ at low current where the modulation is almost total. The current decay $I(t)$ is superimposed

Plotting the N_d of each maximum as a function of $1/\lambda$, we verified a high linearity (0.9999 correlation coefficient in the range $0.3 < \lambda < 0.7$ [μm]). From the slope, we can calculate the experimental value of N_d which is $N_d = 65.3 \pm 0.2$ at $\gamma mc^2 = 240$ MeV and $\lambda = 6238$ Å for a dispersive section gap of 35 mm. This value is close to the value $N_d = 68$ predicted from the

Table 3

Energy [MeV]	Fundamental wavelength [Å]	Measured N_d on the center of the fundamental	Calculated N_d / Measured N_d	$\frac{G_{OK}}{G_{17}}(\pm 6\%)$ (monoenergetic filamentary beam)
234	6238	73 ± 5	1.04	5.4
210		81 ± 5	1.04	6.0
180		89 ± 5	1.04	6.6
150		95 ± 5	1.02	7.0
234	5145	80 ± 5	1.04	5.9
210		87 ± 5	1.04	6.4
180		93 ± 5	1.04	6.9
150		85 ± 5	1.02	6.3

field measurements. The discrepancy could be due to the Hall probe calibration, the storage ring energy calibration, or the error in the calculation of N_d produced by neglecting the cooperation of undulator field and the fringe field of the dispersive section. Note that these values are lower than in Table 2 because the gap is wider.

Fundamental resonance spectra have been taken at four different energies. Results are summarized in Table 3. At each energy the gap was adjusted to center the fundamental around 5000 Å; N_d was then measured by counting the number of fringes from one side to the other of the resonance. Such a measurement is rather imprecise because the envelope variations artificially increase the measured N_d. Values were corrected for this effect and rescaled to the two laser wavelengths 6328 and 5145 Å using the $1/\lambda$ dependence. Those N_d values are then compared to the ones predicted from field measurements. A good agreement (within 2 to 4%) is obtained in a range of field variations of about a factor of 2. Finally the corresponding maximum gain enhancement of the optical klystron over the original 17 periods undulator is calculated for a monoenergetic filament beam (no inhomogeneous broadening).

The following approximate formula has been used [5]:

$$\frac{G_{OK}}{G_{17}} = \left(\frac{14}{17}\right)^3 \times 0.926 \times \frac{N_d}{7}. \tag{4}$$

2.2. Inhomogeneous Broadening

Electrons with different energy, initial angle and initial transverse position produce an emission spectrum shifted in wavelength from that of the ideal electron. The overall measured spectrum no longer presents a complete modulation. Such effects are usually present to some degree (Figs. 4 and 5). The modulation depth f is defined on one period of the fine structure by:

$$f = \frac{x_M - x_m}{x_M + x_m} < 1, \tag{5}$$

where x_m and x_M stand for the minimum and maximum spectral intensity of this period. The modulation depth f may vary as a function of wavelength across the spectrum; $f = 1$ means complete modulation.

When the OK is used as an amplifier, one can show that the bunching and the gain are both proportional to f [5]. It is therefore important to control this parameter if one wants to optimize the gain. The measured modulation f is produced by a number of different physical causes. If these causes are independent (as is predicted for storage rings), the measured f is the simple product of the individual f factors. Namely $f = f_f \times f_m \times f_e$ where f_f is the modulation rate contribution from the OK field imperfection, f_m is due to the monochromator and f_e to the electron beam energy spread, angular spread and transverse dimensions. The monochromator contributes through its angular aperture and bandpass as [4]:

$$f_m = \exp\left[-\left(\frac{\pi}{12}\frac{L+d}{\lambda}a^2\right)^2\right]\frac{\sin^2\alpha}{\alpha^2} \tag{6}$$

with

$$\alpha = \pi(N + N_d)\Delta\lambda/\lambda. \tag{7}$$

Where L and d are the lengths of one undulator and the dispersive section, respectively, a is the total angular aperture of the pinhole and $\Delta\lambda$ the monochromator FWHM. Equation (6) gives $g_m = 0.992$ for our experiment ($a = 4.3 \times 10^{-5}$, $\Delta\lambda = 4$ Å).

Energy Spread. Figure 4 shows a spectrum at 240 MeV and 40 mA of current. The incomplete modulation is

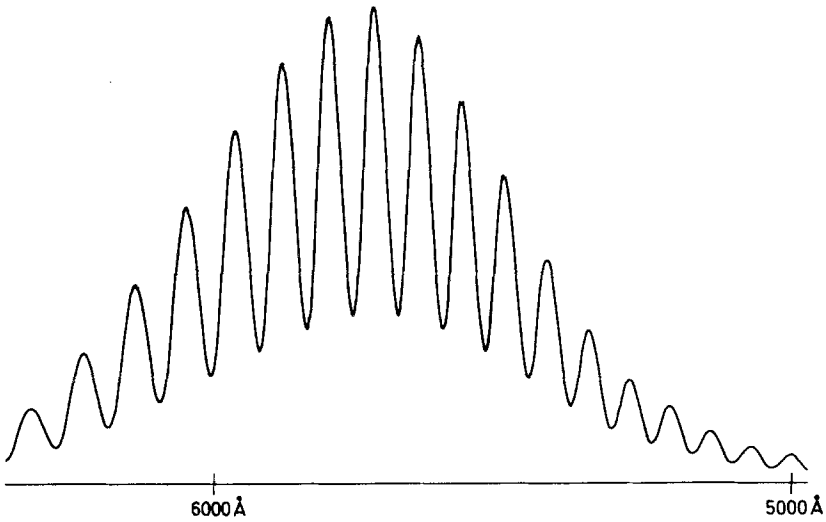

Fig. 4. Spontaneous emission spectrum $dI/d\lambda d\Omega$ measured for an electron energy of 240 MeV, a current of 40 mA and a magnetic gap of 35 mm. The non complete modulation is due to fractional energy spread of 1.2×10^{-3}

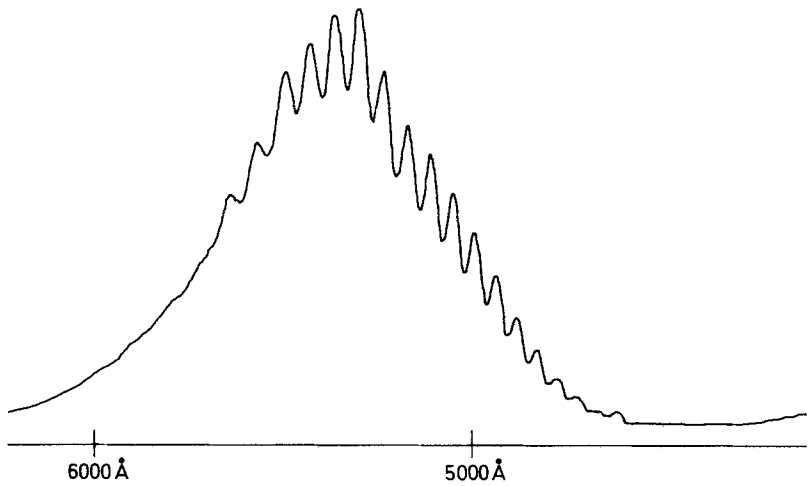

Fig. 5. Spontaneous emission spectrum $dI/d\lambda d\Omega$ measured at low curent and 240 MeV. The modulation is reduced below that of figure 3 by inducing large angular motion in the beam with a broad band noise source applied to an electrode in the vacuum chamber. Note the non-symmetric modulation characteristic of the angular spread as opposed to the symmetric modulation observed in the case of a dominant energy spread (Fig. 4)

attributed entirely to the energy spread in this case for two reasons. All the other contributions are predicted to be negligible as we will see in the next two sections, and the deduced energy spread [5], namely

$$\frac{\sigma_\gamma}{\gamma} = \frac{1}{4\pi(N+N_d)} \sqrt{-2\log f} = 1.2 \times 10^{-3}$$

is consistent with the value $1.4 \times 10^{-3} \pm 0.2$ predicted from the measured bunch length assuming constant synchrotron frequency.

The theory also predicts that for a Gaussian energy spread $f \sim \exp(-\sigma^2/2)$ with $\sigma \propto 1/\lambda$. Calculating for the eleven largest fine structure peaks one verifies the proportionality of σ versus $1/\lambda$ with a correlation coefficient of 0.95. Such a test is not powerful since $1/\lambda$ does not change much inside the bandwidth of the fundamental.

We have also measured f and deduced σ for the first three harmonics recorded at the same energy, current and gap. This data can be used for a more precise check of the λ dependence. Table 4 summarizes the measurements after deconvolution from the monochromator response.

In Table 4 the measured σ is compared to the predicted values from three different energy distribution shapes all normalized the fundamental. We observe a good agreement with the Gaussian energy spread predicted from storage ring theory [9]. The accuracy of this test on the energy distribution depends on the assumption that for a monoenergetic filament beam the modulation rate f is equal to 1. Residual modulation can be produced either by field errors in the OK, or an error in the pinhole positioning with respect to the mirror focal point. We have measured a 0.935 modulation depth at very low current, subtracted all

Table 4

σ	Fundamental	2nd harmonic	3nd harmonic
Measured	0.73 ± 0.01	1.45 ± 0.1	2.09 ± 0.05
Predicted from Gaussian energy spread	0.73	1.46	2.19
Predicted from square energy spread	0.73	1.55	2.68
Predicted from Lorentzian energy spread	0.73	1.35	1.62

the known contributions, and found $f_f \geqq 0.98$ at the fundamental. The assumption is therefore almost satisfied on the fundamental.

Under certain operating conditions, current thresholds exist in ACO at which we have observed sudden rises in energy spread due to longitudinal oscillations of the electron bunch (phase oscillations). At these thresholds we have used the change in modulation rate to measure the energy amplitude of the phase oscillations [5]. Values as high as 1.8×10^{-3} have been recorded. The monochromator output at a wavelength corresponding to a minimum of the fine structure is directly related to the energy spread, and can be used as an energy spread meter. By this method we have measured energy spread variations as small as 2×10^{-5}. The noise limiting the measurement was consistent with that predicted from the storage ring power supply fluctuations. We plan to use this technique in parallel with the bunch lengthening measurement to obtain independent and simultaneous measurements of the energy spread and bunch length changes induced on the beam by an external laser or the FEL itself.

Angular Spread. Electron beam angular spread is also expected to decrease the modulation rate. On the beam axis, the prediction gives:

$$f = [(1+2\sigma_1^2)(1+2\sigma_2^2)]^{-1/4} \tag{8}$$

with

$$\sigma_i = \pi \frac{(d+L)}{\lambda} \sqrt{2}\, \sigma_{\theta i}^2, \tag{9}$$

where the angular distribution is assumed to be Gaussian with horizontal and vertical rms spread σ_{θ_1} and σ_{θ_2}.

At low current at 240 MeV, the theory predicts that $\sigma_{\theta_1} \cong 0.2$ mrad and $\sigma_{\theta_2} \cong 0.1$ mrad implying $f \cong 0.97$. This value drops to $f = 0.93$ at 30 mA of current. The angular effect is rather small, and is usually dominated by the effect of the energy spread. However at minimum current the energy spread contribution $f \cong 0.98$ is on the same order of magnitude as the angular effect. Those low values were experimentally confirmed by the observation of low current modulation depths as high as 0.935.

The angular spread in ACO can be magnified by exciting transverse oscillations in the beam using a broad band noise source applied to an electrode in the vacuum chamber. The on axis spectrum given by Fig. 5 was obtained by this method. Since the energy spread is known to stay constant doing this kind of beam excitation, we attribute the modulation depth degradation to an increase in the angular spread. The curve presents a higher modulation rate on the short-wavelength side than on the long-wavelength side. This asymmetry is very well explained by the fact that the spectrum depends on the square angle θ^2 [5] which is not symmetrically distributed.

Off-axis spectra were also recorded (with the noise source off). Theory predicts the modulation rate to vary quadratically with observation angle

$$f \cong f(\theta_1 = \theta_2 = 0 \exp\left(-\theta_1^2 \frac{\sigma_1^2}{\sigma_{\theta_1}^2} - \theta_2^2 \frac{\sigma_2^2}{\sigma_{\theta_2}^2} \right), \tag{10}$$

where θ_1 and θ_2 are the horizontal and vertical angle between the observation direction and the electron trajectory axis. In (10) we assumed $\sigma_i \ll 1$. From (9 and 10) one has

$$-\lambda^2 \log f = \text{const} + 2\pi^2 (d+L)^2 (\theta_1^2 \sigma_{\theta_1}^2 + \theta_2^2 \sigma_{\theta_2}^2). \tag{11}$$

Equation (11) allows calculation of σ_{θ_1} and σ_{θ_2} by measuring the spectra at different angles. Our results are summarized on Figs. 6 and 7. The curves correspond to the least squares fit of (11) allowing for an error in the determination of the electron axis. We find horizontally $\sigma_{\theta_1} = 0.12 \pm 0.01$ mrad and vertically $\sigma_{\theta_2} = 0.12 \pm 0.005$ mrad with the ACO sextupoles in operation, and where the spreads have been assumed constant along the undulator.

In order to optimize the gain in an oscillator experiment, one needs to optimize the modulation depth by making sure that the cavity axis is very close to the beam axis. Defining the angular aperture $\delta\theta$ as the angle for which the modulation rate drops to $\exp(-1/2) = 0.6$, one has $\delta\theta = \pm 1.1$ mrad for $\lambda = 6328$ Å.

Beam Transverse Dimensions. The beam transverse dimensions are also known to decrease the modulation rate. Assuming the beam to be injected exactly in the center of the dispersive section one has [5], assuming $1 - f \ll 1$,

$$f \cong 1 - 16\pi^2 (N + N_d)^2 (Q_x^2 \sigma_x^4 + Q_y^2 \sigma_y^4), \tag{12}$$

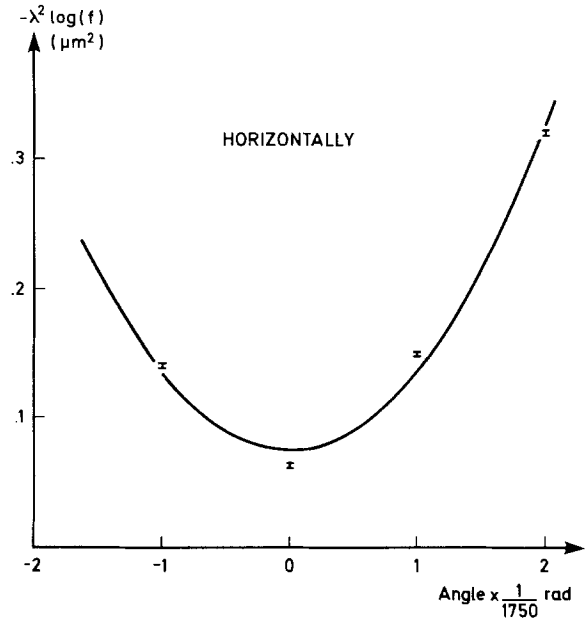

Fig. 6. Effect on the modulation rate of the horizontal angle of observation with respect to the electron trajectory axis. The curve plotted is the least squares fit of $-\lambda^2 \log$ (mdulation rate) to a second order polynomial of the angle. The fit gives the horizontal angular spread σ_θ 0.12 ± 0.01 mrad

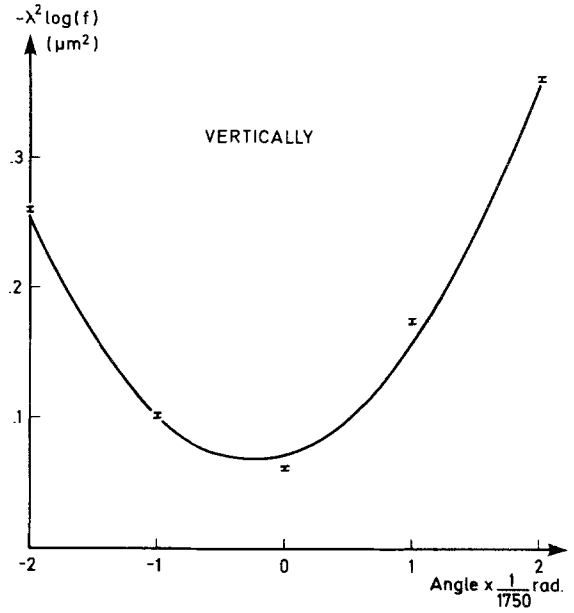

Fig. 7. Effect on the measured modulation rate of the vertical angle of observation with respect to the electron trajectory axis. The fit gives the vertical angular spread $\sigma_\theta = 0.12 \pm 0.005$ mrad

where σ_x and σ_y are the horizontal and vertical rms transverse spreads. Q_x and Q_y are coefficients connected to the field gradients in the dispersive section. They only depend on the field geometry and are equal to zero if the field is exactly uniform. $Q_y \cong 3.4 \times 10^{-4}\,\mathrm{mm}^{-2}$ was deduced from field measurement; this value is just 10% lower than anticipated from the field calculation. These calculations also predicted $Q_x \cong 8.4 \times 10^{-5}\,\mathrm{mm}^{-2}$, a value which has been roughly confirmed by the field measurements. Taking $\sigma_x = \sigma_y = 0.35$ mm (low current) and $\sigma_x = \sigma_y = 0.5$ mm (30 mA of current at 240 MeV) on has $f = 0.9985$ (low current) to $f = 0.997$ (high current). Such a tiny effect was covered experimentally by the energy spread and the angular spread. In some cases, verification may by possible by injecting the electron beam at a distance (x_0, y_0) from the dispersive section axis. Equation (12) still applies if one replaces $\sigma_x^4(\sigma_y^4)$ by $\sigma_x^4 + 2x_0^2\sigma_x^2$ $(\sigma_y^4 + 2y_0^2\sigma_y^2)$. Such an experiment was not possible on ACO because of the change in the beam focussing which would have occurred at the same time. The modulation rate only depends weakly on the injection point in the dispersive section. As in previous subsection one can define the apertures: horizontal aperture: ± 20 mm; vertical aperture: ± 4.7 mm.

2.3. Harmonics

Figures 8 and 9 show the second and third harmonics recorded at 240 MeV and a gap of 32.60 mm at 0.3 mA and 5 mA of current, respectively. As for a regular undulator, an ideal optical klystron does not emit any 2nd harmonic on axis and in fact, the measured peak intensity in Fig. 8 was only 8% of that of the fundamental. This residual intensity is due to the trajectory effect of the fringing fields of the two adjacent bending magnets of ACO. The third harmonic has a shape similar to the first harmonic. Fitting for N to the envelope curve of (3) gives $N = 3.8$ instead of 7. We know from the 3rd harmonic measurements on the 17 periods undulator that inhomogeneous effects are not responsible for this broadening [3]. The dispersive section must therefore be responsible for this effect either via an imperfect compensation or through a destructive interference introduced by the dispersive section at the undulator wavelength.

2.4. Dispersive Section Spontaneous Emission

The dispersive section is equivalent to a three pole wiggler and therefore, has a broad emission spectrum. If one is just interested in the FEL gain improvement, one can ignore the dispersive section intrinsic emission. However, apart from the OK fringes present across all the spectra we have observed (0.2 to 0.7 μm) and apart from the broadening or narrowing of the emission curves (which we have already discussed), there are some unique features which appear in the spontaneous

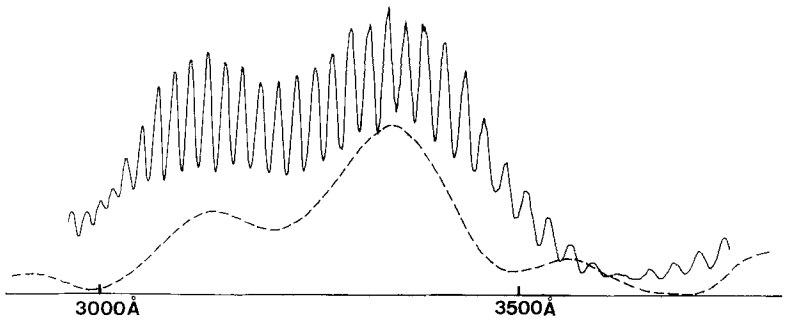

Fig. 8. Second harmonic emission spectrum $dI/d\lambda d\Omega$ at an energy of 240 MeV, 3 mA current, and $K=2.28$. The measured peak intensity is only 8% of the fundamental. The dash line represents the calculated emission of a 7 periods undulator including the fringe field of the nearby ACO bending magnet

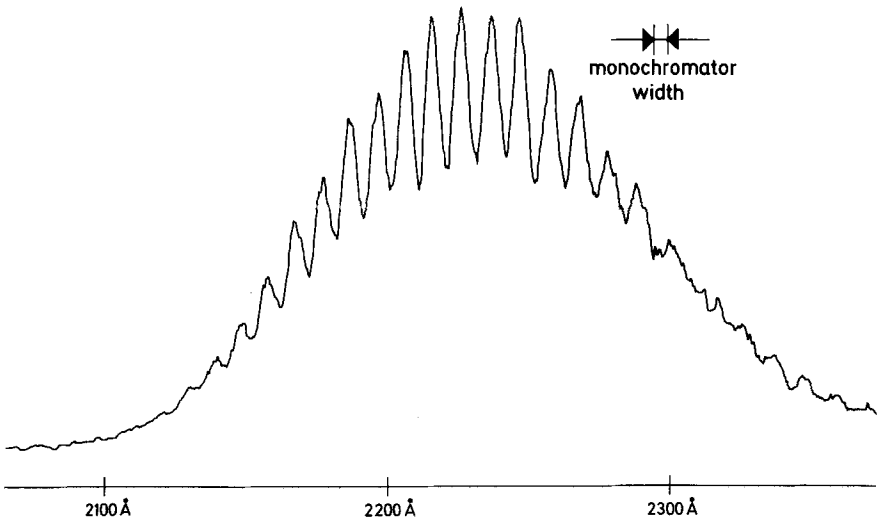

Fig. 9. The third harmonic emission spectrum $dI/d\lambda d\Omega$ at an energy of 240 MeV, 5 mA current, and $K=2.28$. The resonance is broader than expected by a factor 1.5. The modulation is much lower than on the fundamental because of its higher sensitivity to inhomogeneous effects ($N_d(3^{nd}$ harmonic)$\cong 3N_d$ (fundamental)$\cong 220$)

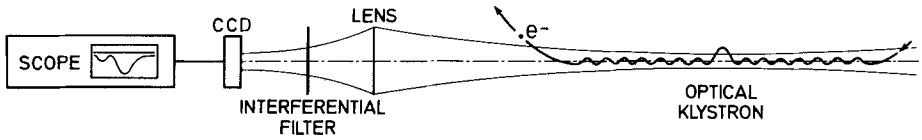

Fig. 10. Experimental set up to display horizontal and vertical profiles of the light emitted by electrons in the optical klystron

emission due to the presence of the dispersive section.

Dispersive Section as a Transversely Displaced Point Source. It is clear from Fig. 1 that a large part of the light emitted by an electron in the dispersive section comes from points that are up to 2 mm away from the undulator axis. This can be observed by refocussing the OK synchrotron radiation. This technique is commonly used on storage rings to image the transverse profile of an electron beam in a bending magnet. Figure 10 shows the experimental set up consisting of a lens (focal length: 1.5 m) located 2.93 m from the center of the dispersive section and a charge coupled device (CCD) exposed through a narrow interference filter ($\lambda=4880$ Å; bandwidth: 12 Å) and placed at 2.24 m from the lens. According to the CCD orientation, vertical and horizontal image profiles were recorded and displayed on a scope. Figure 11a shows a horizontal profile for a 37.85 mm gap at 240 MeV. At this energy and gap, the filter wavelength falls within the on axis fundamental resonance and the profile shows a sharp peak, The gain is set with the peak going off scale in order to make visible the shoulder on the left-hand side. This shoulder remains on Fig. 11b where the central peak was removed by decreasing the gap down to 33.14 mm. We believe that the light profile of Fig. 11b comes from the dispersive section alone. The residual structure is almost unchanged in a gap range sufficient to sweep the filter wavelength across the fundamental resonance.

The shoulder asymmetric with respect to the peak axis is only seen in the horizontal plane (trajectory plane)

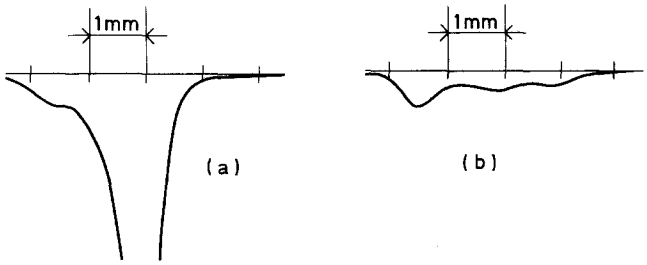

Fig. 11a and b. Transverse horizontal beam profiles of the light emitted by the electrons in the optical klystron. In (a) the interference filter center wavelength falls inside the undulator fundamental resonance; the peak is mainly due to the emission by electrons in the two undulators. The left hand shoulder is mainly due to the emission in the dispersive section. It is still present in (b) where the gap was decreased to suppress completely the undulator emission

and not in the vertical. The peak of Fig. 11b shows maximum definition when the CCD is positioned in the image plane of the dispersive section. This peak corresponds to light emitted from a source displaced about 1.5 mm from the undulator axis as compared to the theoretical 2 mm off axis excursion of the electrons in the dispersive section.

Optical Klystron Emission at Large Gap. At large gap the undulator field vanishes exponentially, much faster than the dispersive section field. The usual coloured ring [7, 6, 2] due to the interference of light from the undulator periods vanish. However one still sees a double interference structure centered about the undulator axis. A black and white reproduction is given in Fig. 13 for the gap series {142, 121, 182 mm} at 240 MeV. The dispersive section maximum field is {660, 1150, 1570 Gauss}, more than 20 times larger than the undulator peak field. This emission is not due to the undulator but is produced by the dispersive section with some contribution from the storage ring bending magnets fringe field.

The emission produced in the dispersive section is contained within the maximal tangent directions labeled A and B in Fig. 12a. At large distances the radiation pattern is symmetric about the axis 0. Schematically, due to the small $1/\gamma$ emission cone, an observer in the electron orbit plane between 0 and A will see the emission of the $t_1 - t_2$ part of trajectory shown in Fig. 12b. In the θ direction with respect to A, the emission is mainly due to small regions around tangent points t_1 and t_2 where the curvature is important (between t_1 and t_2 the curvature is very small and the emission of this part of trajectory can be neglected). Both points sources t_1 and t_2 interfere constructively when the difference in electron and photon transit times is an integral number of optical

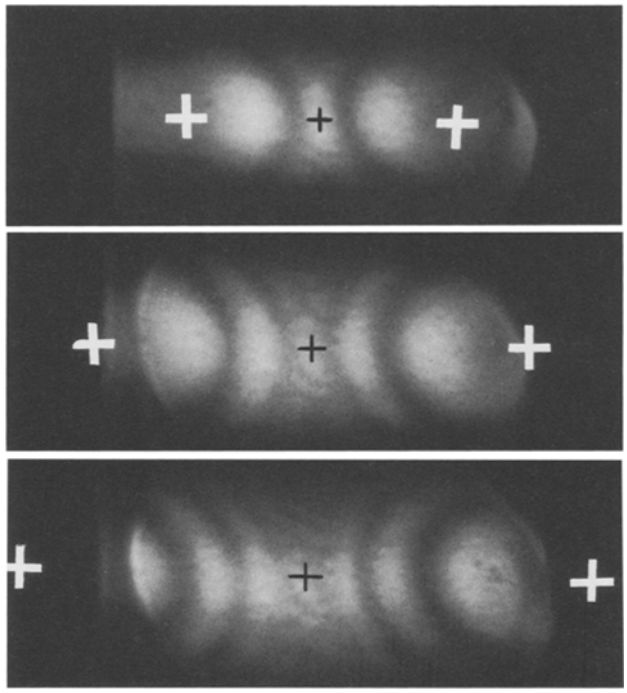

Fig. 13. Three photographs filtered at 5500 Å of the interference structure produced in the optical klystron at large gap. From top to bottom, the magnetic field is increased by closing the gap. The beam axis is marked by the black cross at the center of each pattern, and the points A and B calculated from the magnetic field strength in the OK are marked with white crosses

periods:

$$n\frac{\lambda}{c} = \int_{t_2}^{t_1} \frac{\delta s}{\beta c} - \frac{d}{c} \cong \frac{d}{2c\gamma^2}(1+\gamma^2\theta^2), \tag{13}$$

where d is practically half of dispersive section length and n is an integer.

For monochromatic light the interference maxima occur at a constant angle θ tracing out circles around A in the observation plane. Of course, the circles are incomplete because the angle of emission goes outside the electrons $1/\gamma$ forward cone, where the intensity drops to zero. The same interference pattern occurs around B direction, and one sees a double colored interference structure centered on A and B directions as illustrated in Fig. 13, for $\lambda = 5500$ Å and $E = 240$ MeV. Positions in fringe are in a rather good agreement with theoretical values calculated from (13), where $d \cong 8$ to 10 cm, the angle of A direction being 3.6 mrad, 6 mrad and 7.9 mrad, respectively, for each photographs.

Patterns like Fig. 13 have been recorded at 240, 540 MeV, and several different gaps. As the magnetic field in the dispersive section is increased by reducing the gap, the A–B angle increases, and more interference bands become visible. At small gap, the usual

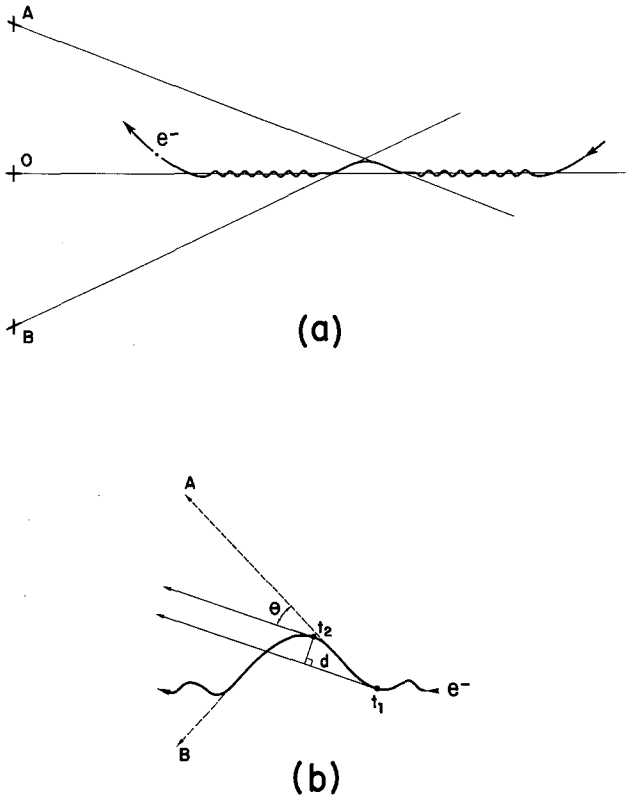

Fig. 12. (a) Sketch of the electron orbit in the optical klystron showing the axis 0 and the maximal emission angles A and B. The scale of the wiggles in the undulator is greatly exaggerated for clarity. (b) Detail of electron orbit in the dispersive section showing the two emission points t_1 and t_2 and the interference between them. The total angular field where the fringes exist is of the order of 15 mrad for our experiments on ACO at 240 MeV

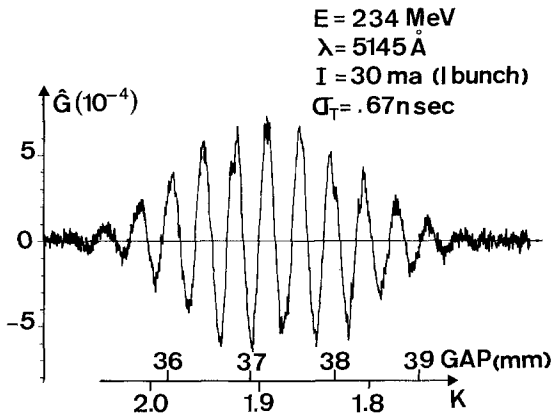

Fig. 14. Gain profile versus magnetic gap measured on an argon laser at $\lambda = 5145$ Å with one electron bunch of 30 mA of current a 234 MeV. The peak gain is calculated using an rms bunch length measured to be $\sigma_l = 0.67$ ns. As predicted from Madey's theorem, this curve is proportional to the derivative of the spontaneous emission curve 15 (b) taken under similar conditions

undulator ring pattern appears superimposed on the klystron interference structure, and eventually the undulator intensity totally dominates the other radiation sources.

Interference between the emission in the bending magnets' fringe field is observed on axis when the undulator and klystron emission is reduced to a low level. This effect produces a small concentric ring structure [11] centered between the white rings produced by the bending magnets individually.

3. Gain

We have measured the gain experienced by an external argon laser aligned colinear with the electron beam inside the optical klystron. The experimental method is identical to that used with the undulator and has already been described [12, 13, 6]. A typical gain profile as a function of the gap is shown in Fig. 14.

Since both the dispersive section gap and the undulator gap are scanned at the same time due to the construction of the optical klystron all magnetic field strengths vary as a function of the gap. The K parameter of the undulators and the N_d parameter of the dispersive section vary at different rates due to the different geometries of the respective structures. If N_d were constant, the gain would trace out the envelope as a function of the gap of the undulator with no rapid oscillations. If the K parameter were constant, the envelope would be flat and the gain would oscillate rapidly as a function of the gap of the dispersive section. In fact both N_d and K change together producing the observed curve. The number of peaks observed inside the envelope depends only on the rate of change of N_d and K as a function of gap.

Figure 15 compares the spontaneous emission curves taken as a function of wavelength and gap. The respective theoretical envelopes are superimposed on each curves. The local rate of change of N_d as a function of magnetic field can be deduced from the lower curves; it is clearly lower than the rate of change as a function of wavelength. Unfortunately, edge and end effects play a dominant role in determining the amplitude of the field in the dispersive region so that the field is not related to the gap via a simple exponential. Madey's theorem [8] implies that the gain curve taken as a function of gap as shown in Fig. 14 is proportional to the derivative of the spontaneous emission spectrum as a function of gap as shown at the bottom of Fig. 15, where terms of the order N/N_d are neglected. This behaviour is clearly borne out by the data.

The expected optical klystron maximum peak gain $\hat{G}_{ok}$ is equal to [5]:

$$\hat{G}_{ok} = \frac{G_{ok}}{G_{17}} f \hat{G}_{17}, \tag{14}$$

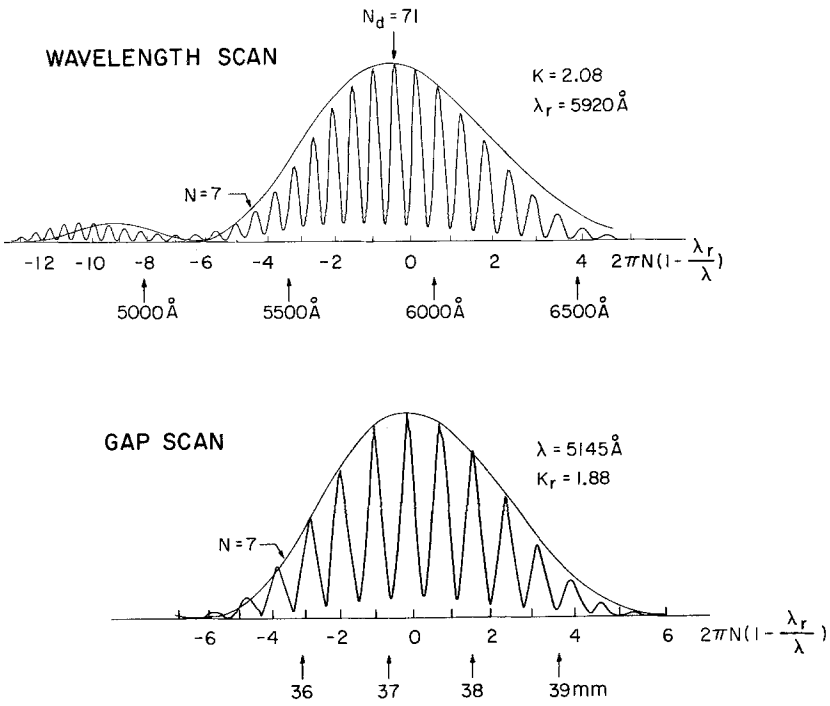

Fig. 15. The spontaneous emission spectrum as a function of wavelength and undulator gap or magnetic field are compared. The rapidly oscillating measured curves fit well into the theoretically calculated envelope curves with some small deviations in the case of the wavelength scan. The slower dependence of the dispersion parameter N_d on gap is visible in the lower curve. The gain as a function of gap is approximately the derivative of the gap scan, not the wavelength scan

where G_{ok}/G_{17} is the OK gain improvement with respect to the original 17 period undulator for a *monoenergetic filament beam*. It is given by (4); see also Table 3.

As before, f is the modulation rate and $\hat{G}_{17}$ is the 17 period undulator peak gain which is equal to [17]

$$\hat{G}_{17} = 1.5 \times 10^{-12} \frac{\lambda_0^2 N^3}{\gamma^3} K^2 [JJ]^2 \varrho_e F_f , \tag{15}$$

where λ_0 is the undulator period in cm, $[JJ]^2$ is the Bessel function factor [13]. $K = eB\lambda_0/2\pi mc$ is the peak field magnetic parameter, ϱ_e the peak electron density in cm^{-3}, and F_f is the filling factor which can be calculated from the overlap integral between the electron and laser beams. For coaxial weakly diverging beams [14].

$$F_f = \frac{1}{\sqrt{\left[1+\left(\frac{w_0}{2\sigma_h}\right)^2\right]\left[1+\left(\frac{w_0}{2\sigma_v}\right)^2\right]}} , \tag{16}$$

where w_0 is the laser beam waist and σ_h and σ_v the electron beam transverse rms sizes.

The theoretical peak gain predicted for the measurement shown on Fig. 14 is

$$(\hat{G}_{ok})_{th} = 4.0(\hat{G}_{17})_{th} = 6.6 \times 10^{-4} \pm 30\% \tag{17}$$

with $G_{OK}/G_{17} = 5.9$ (Table 3), $f = 0.67$ (measured on the spontaneous emission) and $(\hat{G}_{17})_{th}$ calculated from (15, 16). The 30% error bars originate primarily from the uncertainty in the β functions in the undulator. The measured peak gain is (Fig. 14):

$$(\hat{G}_{ok})_{meas} = 7\ 10^{-4}(\pm 0.3) . \tag{18}$$

The agreement between the theoretically predicted (17) and measured (18) values is remarkably good, and certainly the best achieved to date. This was made possible by improvements in the alignment technique, and by thorough characterisation of the laser mode. Not only does the values of he gain reported here confirm the validity of the theory, but it also represents a large increase over the gain measured with the undulator NOEL.

4. Bunch Lengthening

Bunch lengthening experiments have been performed by superposing an argon laser colinear with the electron beam inside the optical klystron. The experimental set up has already been described [10, 3], good agreement was observed with stochastic heating models [15] at very low current while high current regimes are dominated by anomalous bunch lengthening effects. Figure 16 shows the bunch lengthening and spontaneous emission produced by the optical klystron. The vertical line indicates an undulator parameter K of 1.92. The results are in good agreement with the theorem demonstrated by Madey that the mean squared energy spread is proportional to the spontaneous power spectrum [8].

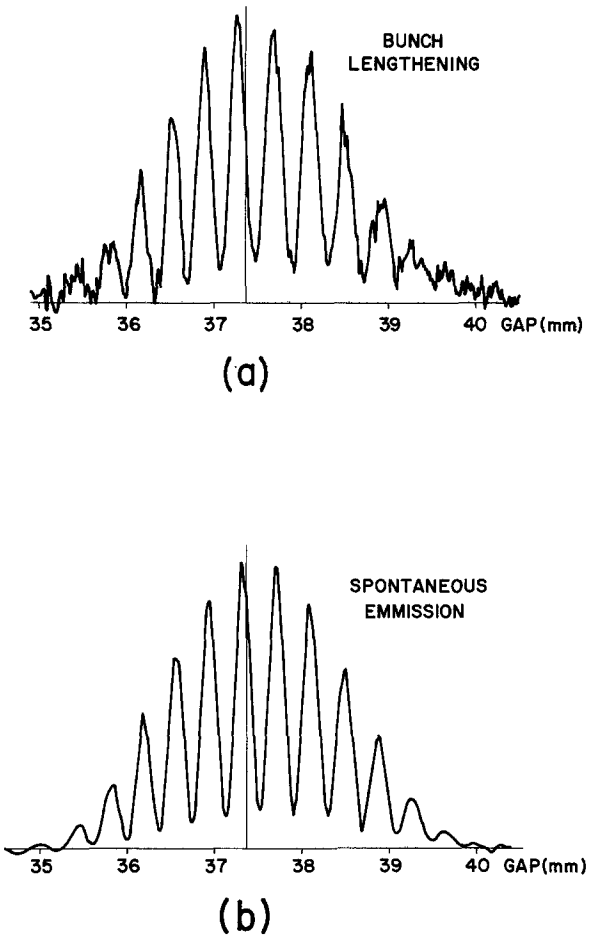

Fig. 16a and b. Laser induced bunch lengthening (a) and spontaneous emission (b) as a function of magnetic gap in mm. As predicted from Madey's second theorem bunch lengthening is proportionnal to the spontaneous emission. The vertical scale of figure a depends on experimental conditions. At very low current typical bunch lengthening of 4% are observed for $K = 1.92$

The peak low current lengthening produced by the OK was measured to be 0.67 of that of the undulator. As expected, this reduction factor is quite close to the square of the ratio of the number of periods $(14/17)^2$. We have clearly succeeded in constructing a device which provides at the same time more gain and less beam heating than an undulator.

5. Conclusion

Our tests of the performance of an optical klystron have been successful. We have increased the single-mode peak gain by a factor of four to the optimum value, for ACO, set by the energy spread of the stored beam. The low current bunch lengthening scaled as expected by the simple theory. The installation of this device was the crucial factor which permitted the recent operation of the ACO storage ring laser above threshold [18].

During the course of this work, we have been able to verify the performance of the klystron through a variety of means. The spontaneous, gain and bunch lengthening spectra as a function of wavelength and gap have been measured and found to be in agreement with our theoretical calculation. The dependance of the modulation depth of the spontaneous spectrum on electron beam quality has also been used to measure the energy spread and emittance of the stored beam.

Acknowledgements. The authors are greatly indebted to the technical team of the LURE laboratory for much help. Also they thank the storage ring people of the LAL for fruitful discussions and the "Service Aimant" of the LAL for experimental help. This work was supported in part by the AFOSR contract F49420-80-C 0068, the DRET contract 81/131, the CEN Saclay DPC/SPP/SP and the CNRS, and was performed in part by Deacon Research under contract to Stanford University.

References

1. J.M. Ortega, C., Bazin, D.A.G. Deacon, C. Depautex, P. Elleaume: Nucl. Instrum. Methods **206**, 281 (1983)
2. J.M. Ortega, C. Bazin, D.A.G. Deacon: J. Appl. Phys. **54**, 4776 (1983)
3. M. Billardon, D.A.G. Deacon, P. Elleaume, J.M. Ortega, K.E. Robinson, C. Bazin, M. Bergher, J.M.J. Madey, Y. Petroff, M. Velghe: Recent results of the ACO Storage ring FEL experiment, Proc. Bendor Free Electron Laser Conference, ed. by M. Billardon and D.A.G. Deacon, J. Phys. (Paris) **44**, C1–29 (1983)
4. N.A. Vinokurov, A.N. Skrinsky: Preprint INP 77–59, Novosibirsk (1977); see also N.A. Vinokurov: Proc. 10th Intern. Conf. High Energy Charged Particle Accelerators, Serpukhov, Vol. 2 (1977) p. 454
5. P. Elleaume: Optical Klystrons, Proc. Bendor Free Electron Laser Conference, ed. by M. Billardon and D.A.G. Deacon, J. Phys. (Paris) **44**, C1–353 (1983)
6. C. Bazin, M. Billardon, D.A.G. Deacon, P. Elleaume, Y. Farge, J.M.J. Madey, J.M. Ortega, Y. Petroff, K.E. Robinson, M.F. Velghe: Results of the First Phase of the ACO Storage Ring Laser Experiment in *Physics of Quantum Electronics* Vol. 8, ed. by S.F. Jacobs, G.T. Moore, H.S. Pilloff, M. Sargent III, M.O. Scully, R. Spitzer, (Addison-Wesley, Reading, MA 1982) p. 89
7. C. Bazin, M. Billardon, D.A.G. Deacon, Y. Farge, J.M. Ortega, J. Perot, Y. Petroff, M. Velghe: J. Phys. Lett. **41**, 547 (1980)
8. The original derivation of the theorems is due to J.M.J. Madey, Nuovo Cimento **B50**, 64 (1979), an experimental verification is in [13]. A more general proof is given by N.M. Kroll in *Physics of Quantum Electronics* (1982) p. 315, and other derivations are available in N.A. Vinokurov and A.N. Skrinsky, Preprint INP 77–59, Novosibirsk (1977), S. Krinsky, J. Wang, P. Luccio Brookhaven National Laboratory, BNL Report 30425 R (March 1982)
9. M. Sands: SLAC Report No. 121 (Stanford Linear Accelerator Center, Stanford, CA 1970)

10. K.E. Robinson, D.A.G. Deacon, M.F. Velghe, J.M.J. Madey: IEEE J. QE-**19**, 365 (1983)
11. M.M. Nikitin, A.F. Medvedev, M.B. Moiseev: Sov. Tech. Phys. Lett. **5**, 347 (1979)
12. D.A.G. Deacon, J.M.J. Madey, K.E. Robinson, C. Bazin, M. Billardon, P. Elleaume, Y. Farge, J.M. Ortega, Y. Petroff, M. Velghe: IEEE Trans. NS-**28**, 3142 (1981)
13. D.A.G. Deacon, K. Robinson, J.M.J. Madey, C. Bazin, M. Billardon, P. Elleaume, Y. Farge, J.M. Ortega, Y. Petroff, M. Velghe: Opt. Commun. **40**, 373 (1982)
14. P. Elleaume, D.A.G. Deacon: Appl. Phys. B**33**, 9 (1984)
15. A. Renieri: IEEE Trans. NS-**26**, 3827 (1979).
L.R. Elias, J.M.J. Madey, T.I. Smith: Appl. Phys. **23**, (1980)
C. Pellegrini: IEEE Trans. NS-**26**, 3791 (1979)
D.A.G. Deacon: Appl. Phys. **19**, 97 (1979)
16. J. Schwinger: Phys. Rev. **75**, 1912 (1949). The calculations are well detailed by J.D. Jackson, *Classical Electrodynamics*, 2nd ed. (Wiley, New York 1900) Chap. 14
17. W.B. Colson: Ph. D. Thesis, Standford University (1977)
18. M. Billardon, P. Elleaume, J.M. Ortega, C. Bazin, M. Bergher, M. Velghe, Y. Petroff, D.A.G. Deacon, K.E. Robinson, J.M.J. Madey: Phys. Rev. Lett. **51**, 1652 (1983)